Received November 7, 2017, accepted January 26, 2018, date of publication February 5, 2018, date of current version March 15, 2018.

*Digital Object Identifier 10.1109/ACCESS.2018.2802447*

# Soft Iterative Quantum Receivers Approaching the Helstrom Limit Using Realistic Quantum Devices

**CHENJIA WEI[1], XIAOLIN ZHOU[1], (Member, IEEE), LINGDA WANG[2], PENGFEI TIAN[3], (Member, IEEE), AND LAJOS HANZO[4], (Fellow, IEEE)**

[1]Key Laboratory for Information Science of Electromagnetic Waves, School of Information Science and Technology, Fudan University, Shanghai 200433, China
[2]Department of Electrical and Computer Engineering, University of Illinois at Urbana–Champaign, Urbana, IL 61801, USA
[3]Engineering Research Center of Advanced Lighting Technology, Ministry of Education, Institute for Electric Light Sources, Fudan University, Shanghai 200433, China
[4]Communications, Signal Processing and Control Group, School of ECS, University of Southampton, Southampton SO17 1BJ, U.K.

Corresponding author: Xiaolin Zhou (zhouxiaolin@fudan.edu.cn)

This work was supported in part by the National Natural Science Foundation of China under Grant 61571135, in part by the Shanghai Sailing Program under Grant 17YF1429100, and in part by the State Key Laboratory of Intense Pulsed Radiation Simulation and Effect Funding. The work of L. Hanzo was supported by the European Research Council through the Advanced Fellow Grant.

**ABSTRACT** One of the most crucial challenges in quantum communication is the discrimination of the non-orthogonal coherent states approaching the Helstrom limit. In this paper, a soft iterative quantum receiver is derived for discriminating among the coherent states. The receivers employing the iterative strategy for optimizing the feedback measurement are capable of operating closer to the theoretical error probability limit, actuating about 1.05 dB improvement over a recent proposed quantum receiver. The iterative quantum receivers achieve excellent performance despite using a reduced number of feedback measurement steps. Monte Carlo simulations are performed for quantifying the influence of practical quantum-domain impairments. These results suggest that iterative detection offers substantial robustness against many imperfections degrading realistic experimental implementation.

**INDEX TERMS** Quantum communications, soft iterative quantum receiver, Helstrom limit, quantum-domain impairments, robustness.

## I. INTRODUCTION

The laws of quantum mechanics provide a promising solution to our quest for miniaturization and increased processing power [1], while quantum information transmission is becoming one of the most promising topics in the field of communications. Coherent states are the best known information carriers in quantum communication owing to their robustness [2]. High-confidence identification of the coherent states in the face of the inherent quantum effects to approach the ultimate physical limit is of both practical and theoretical interest [3].

Binary coherent state discrimination has been theoretically treated and experimentally tested [4]–[8], which has also been shown to outperform the error probability limit of classical receivers that was referred to as the standard quantum limit (SQL) [9]. Indeed they have also been shown to approach the limit of quantum receivers termed as the Helstrom limit (HL) [10]. More recently, in the case of $M$-ary communications, the feedback-aided optimized strategies of [11] and [12] have achieved a theoretical error probability below the SQL. The quantum receiver of [13] is a hybrid scheme amalgamating both the homodyne detector [14] and optimized displacement receiver [15] that carries out a pair of successive measurements. Another quantum receiver designed for $M$-ary communications [16] has a hybrid structure relying on the phase shift and the optimized displacement based receiver. These receivers all utilize the classic Bayesian rules to update the feedback signals. However, these two types of optimized displacement receivers require different quantum states to feed back, which is too complex. Moreover, at the time of writing, there is still a gap between the error probability achieved by the aforementioned non-iterative receivers designed for $M$-ary communication and the HL.

The photon number-resolving detector (PNRD) has been routinely applied for coherent states discrimination to carry

out a generalized measurement, leading to an inconclusive result [17]. The benefit of invoking the PNRD for $M$-ary coherent states discrimination was also intimated in [18], which was shown to be superior to the conventional ON-OFF detector. In practice, the non-ideal quantum efficiency and the dark count of the photon detector, the non-ideal transmittance of the beam splitter as well as the mode mismatch between the signal and the local oscillating field will degrade the performance of the quantum receiver [16]. Investigating the impact of each imperfection separately by numerical simulations allows us to quantify their individual impact [19].

Against this background we propose a novel quantum receiver, which relies on a sequence of feedback measurements optimized by a new iterative strategy. More explicitly, our novel contribution mainly lies in the conception of an efficient iterative *a posteriori* probability (APP) soft demapping strategy conceived for an $M$-ary quantum receiver. The technique proposed in aforementioned paper uses the classic Bayesian updating procedure in each subsequent detection. By contrast, in our approach, we conceived an iterative detection feedback block, which is activated during each subsequent detection iteration. The soft log-likelihood ratio (LLR) of each information bit is used for choosing the specific state for optimizing the feedback to the local oscillating field for the subsequent detection and demodulation. Hence the key contributions of this paper can be summarized as follows:

(1) the proposed iterative receiver exceeds the sensitivity of the recently proposed non-iterative receivers of [20] and [21] and approaches the HL;
(2) the iterative receiver achieves an outstanding error performance at a reduced number of feedback steps, when compared to the conventional non-iterative receiver;
(3) the iterative receiver exhibits robustness to the imperfections of the realistic quantum devices, for example the fidelity degradation due to dark counts.

In a nutshell, the goal of this paper is to provide a characterization of the proposed iterative scheme. The remainder of this paper is organized as follows. In Section II, we outline our notations and formally characterize the coherent states of $M$-ary quadrature amplitude modulation (QAM) signals. In Section III, we introduce the schematic based on 4QAM in simple words to make the paper easier to read both by physicists and engineers. A detailed receiver model and the proposed iterative strategy is then derived for $M$-ary QAM. In Section IV, simulations are provided for characterizing the performance of the iterative receiver both for 4QAM and 16QAM, compared to the recently proposed non-iterative receiver of [20] and [21]. The robustness of the receiver is also discussed in the face of several imperfections including the sub-unity mode mismatch between the signal and the local oscillating field [22], the non-ideal transmittance of the beam splitter [20], the non-ideal quantum efficiency and non-zero dark count of photon detectors [23]. Moreover, we use EXtrinsic Information Transfer (EXIT) charts [24] for analyzing the convergence of the iterative quantum receiver. Section V offers our simulations, our discussions on the performance of the iterative receiver and provides our conclusions.

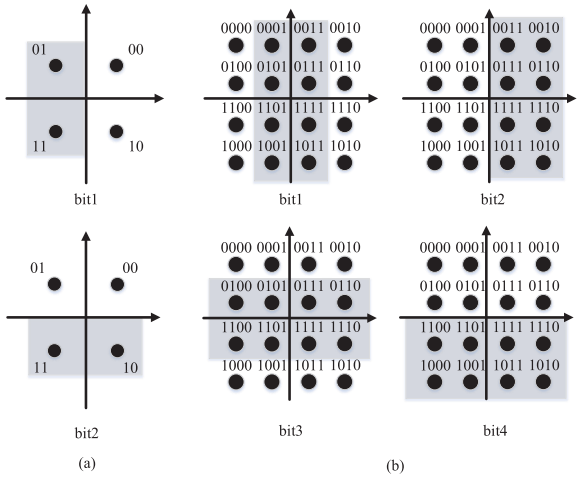


**FIGURE 1.** The subset partitioning for each of the two or four bit position of (a) 4QAM or (b) 16QAM coherent state constellations. The numbers above the constellations point represent the binary information bit. The shaded regions correspond to the decision regions for $x_i = 1$ and the unshaded region correspond to $x_i = 0$.

## II. NOTATIONS AND DEFINITIONS

In quantum detection theory, the information is mapped both to amplitude and phase for QAM signals relying on coherent states. QAM signals can be characterized by a pair of quadrature amplitudes $\hat{x}_c$ and $\hat{x}_s$, which are defined as:

$$\hat{x}_c \equiv (\hat{a} + \hat{a}^\dagger)/2, \quad \hat{x}_s \equiv (\hat{a} - \hat{a}^\dagger)/2i, \tag{1}$$

where $\hat{a}$ and $\hat{a}^\dagger$ denote the annihilation and the creation operators respectively, while $i = \sqrt{-1}$. These amplitudes can be determined independently. When each of the two amplitudes takes $L$ values, the total number $M$ of the signals is represented by

$$M = L^2, \quad L = 3, 4, 5, \cdots. \tag{2}$$

For convenience, the QAM alphabet index set $\Omega$ is defined as follows:

$$\Omega = \{-(L-1) + 2(l-1) \mid l = 1, \cdots, L\}. \tag{3}$$

Using the index above, the QAM signals can be defined as a set of coherent states:

$$\left|\psi_{Sig.\omega}\right\rangle = \left|n_{Sig}(\omega_p + i\omega_q)\right\rangle, \quad \omega_p, \ \omega_q \in \Omega, \tag{4}$$

where $n_{Sig}$ is the average number of photons of the signal and $\omega$ represents the index of the signal, which is related to $\omega_p$ and $\omega_q$. The 4QAM scheme encodes each of the two information bits $x_1x_2$ into $M = 4$ different signals and the 16QAM scheme encodes each of the four information bits $x_1x_2x_3x_4$ into $M = 16$ different signals.

As shown in Fig. 1, the subset partitioning of the 4QAM and 16QAM coherent state constellations for each two bits or four bits is depicted. The shaded regions (only shown

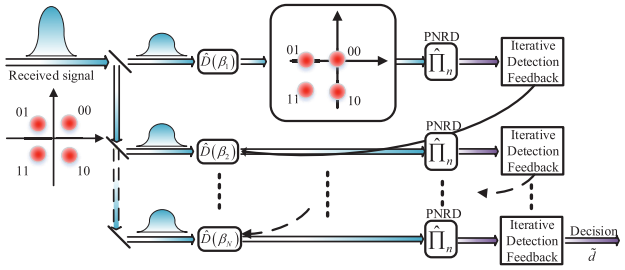


**FIGURE 2.** The receiver splits the received 4QAM signal into $N$ parts. Quantum state after splitting is displaced by $\hat{D}(\beta_j)$ and then measured by a PNRD. Via iteration and feedback control, the value of displacement $\hat{D}(\beta_j)$ in each part depends on the output of iterative detection feedback block.

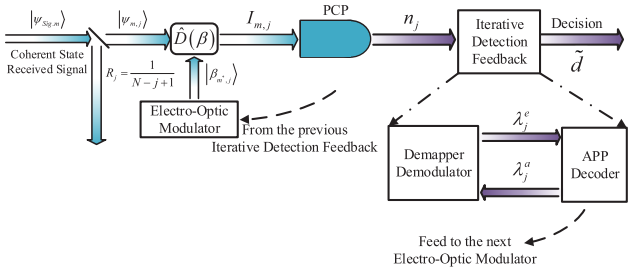


**FIGURE 3.** The schematic of the soft iterative quantum receiver for $j$th measurement approach. The diagonal lies at the input represent the beam splitters, $\hat{D}(\beta)$ is the displacement operate and the PCP represents the photon-counting process using the PNRD. The result of detection $n_j$ is send to iterative detection feedback for iterative demapping and decoding. A final decision $\tilde{d}$ is performed considering the outcomes obtained on the N different parts.

inside the unit square) correspond to the decision regions for each bit in $x_i = 1$, while the unshaded region to $x_i = 0$. Observe in Fig. 1 that the 4QAM constellation is translated to a binary signalling selected from two possible pairs, while the 16QAM constellation is translated to a binary signalling selected from eight possible pairs.

## III. ITERATIVE QUANTUM RECEIVER

In this section, the model of the iterative quantum receiver is derived. The relevant basic iterative detection principles are detailed in a tutorial style in [25]. The receiver has four main components: beam splitters, displacement operations, PNRD and iterative decoders. To present the underlying principle of our iterative quantum receiver, we consider the simple case of 4QAM, as shown in Fig. 2.

Once a quantum state is observed, it is collapsed to a certain classical state. In order to distinguish the information carried by the state, beam splitters can be utilized to split the state, during which the amplitude of the state is reduced but the phase information remains on each split state. The received coherent state 4QAM signal is split into $N$ equal-amplitude parts by $(N-1)$ beam splitters. In our scheme we test the hypothesized state $|\beta_j\rangle$ selected from the 4QAM alphabet and then the input signal is displaced by the displacement operation $\hat{D}(\beta_j)$, invoked for shifting the amplitude to the vicinity of the vacuum state $|0\rangle$. Following this displacement, the signal is detected by the PNRD and the output of the detector is forwarded to the iterative decoders for the iterative feedback process. Prior to the displacement, the signal is delayed to synchronize the iteration and feedback actions. Again, our scheme relies on the iterative strategy using the soft log-likelihood ratios for optimizing the feedback measurement and for decoding the received signals. After each iteration, we estimate the most likely new state $\hat{D}(\beta_{j+1})$ to be tested in the subsequent feedback period using the soft LLR based on the detection and displacement history. The final determination of the input signal state corresponds to the most likely state determined during the last iteration.

### A. ITERATIVE RECEIVER FOR 4QAM

As shown in Fig. 3, the $j$th measurement approach of Fig. 2 for a coherent 4QAM state is demonstrated, which shows the structure of the beam splitter, displacement operation, electro-optic modulator, demapper/demodulator and of the *a posteriori probability* (APP) decoder block in detail. We ensure that the *a priori* probability of the coherent states is the same, i.e., $P_m = 1/4$. Each received signal is split into $N$ parts using $(N-1)$ beam splitters, so that the signal intensity is the same in each part. The $j$th splitting ratio $R_j$ of the signal is $\frac{1}{N-j+1}$ and the corresponding signal is

$$|\psi_{m,j}\rangle = \left|\frac{\psi_{Sig.m}}{\sqrt{N}}\right\rangle, \quad j = 1, \ldots, N, \tag{5}$$

where $m$ is the 4QAM alphabet index. Let us now define the ratio $R = N/M$ to describe the number of split signals and the order of incoming signal. For a large ratio, the number of measurements related to the state will increase, but the signal energy of each measurement becomes low. In other words, we obtain $N$ copies of a weaker state $\left|\frac{\psi_{Sig.m}}{\sqrt{N}}\right\rangle$ of the incoming signal $|\psi_{m,j}\rangle$ without loss of the carried information.

At each part, the displacement operation $\hat{D}(\beta)$ applied to the signal is accomplished by a local field $|\beta_{m^*,j}\rangle$ as

$$D(\hat{\beta})\,|\psi_{m,j}\rangle\,|\beta_{m^*,j}\rangle = |\psi_{m,j} - \beta_{m^*,j}\rangle. \tag{6}$$

It is widely exploited that $D(\beta)$ is realized by a beam splitter leaving a transmittance of $\tau \approx 1$. If $j = 1$, the local field obeys $|\beta_{m^*,1}\rangle = \left|\frac{\psi_{Sig.1}}{\sqrt{N}}\right\rangle$. If $j > 1$, the local field $|\beta_{m^*,j}\rangle$ and $m^*$ are decided by the iterative strategy to be introduced.

Considering the overlapping areas between $|\psi_{m,j}\rangle$ and $|\beta_{m^*,j}\rangle$, the average intensity of each field is [15]

$$I_{m,j} = (1-\xi)\,\tau\,\|\psi_{m,j}\|^2 + \xi\,\|\sqrt{\tau}\psi_{m,j} - \beta_{m^*,j}\|^2, \tag{7}$$

where $\xi, 0 < \xi \leq 1$ represents the effect of mode mismatch and $\tau, 0 < \tau \leq 1$ describes the transmittance of the beam splitter. The contributions [13], [23] showed that the optimal displacement minimizing the error probability was displacing the coherent state signal close to the vacuum state $|0\rangle$.

The photon counting process (PCP) of Fig. 3 is implemented using the PNRD. Following the displacement operation, the number of photons $n_j$ is detected by the PNRD. The measurement operator $\hat{\Pi}_n$ of the PNRD based on $n$-photon

detection was modelled by *Izumi et al.* as [12]

$$\hat{\Pi}_n = e^{-\nu} \sum_{l=0}^{n} \sum_{k=n-l}^{\infty} \frac{\nu^l}{l!} C_{n-l}^{k} \eta^{n-l} (1-\eta)^{k-(n-l)} |k\rangle \langle k|, \quad (8)$$

where $C_{n-l}^{k}$ is the binomial coefficient. If the input signal state is $|\psi_m\rangle$, the signal state after nulling becomes $|\gamma_m\rangle = \left|\frac{\psi_m - \beta_{m^*}}{\sqrt{N}}\right\rangle$. Each split state is measured independently from each other by PNRD with quantum impairments. The probability of detecting $n_j$ photons is given by [26]

$$P\left(n_j|\gamma_m\right) = \langle\gamma_m| \hat{\Pi}_n |\gamma_m\rangle = e^{-\|\gamma_m\|^2} \frac{\left(\|\gamma_m\|^2\right)^{n_j}}{n_j!}, \quad (9)$$

where $\langle\gamma_m| \hat{\Pi}_n |\gamma_m\rangle$ represents the inner product of the bar vector $\langle\gamma_m|$, of the measurement operator $\hat{\Pi}_n$ and of the ket vector $|\gamma_m\rangle$.

The *a posteriori* probability after detecting $n_j$ photons in the $j$th interval is given by [27]

$$P_{post\_m,j} = \frac{P_{prior\_m,j} \cdot P_{m,j}}{\sum_{i=0}^{3} P_{prior\_i,j} \cdot P_{i,j}}, \quad (10)$$

where $P_{prior\_m,j}$ represents the *a priori* probability, and yields

$$P_{prior\_m,j} = P_{prior\_x_1,j} \cdot P_{prior\_x_2,j}, \quad (11)$$

where $P_{prior\_x_1,j}$ and $P_{prior\_x_2,j}$ represent the *a priori* probability of bit $x_1$ and $x_2$, respectively. For the PNRD detector of Fig.3, the probability $P_{m,j}$ in (10) is [28]:

$$P_{m,j} = e^{-\nu-\eta I_{m,j}} \frac{\left(\nu + \eta I_{m,j}\right)^{n_j}}{n_j!}, \quad (12)$$

where $\eta$ describes the quantum efficiency and $\nu$ represents the dark count of the PNRD detector. For an ideal photon detector, the vacuum state is always determined with no error, while misdetection may occur in the other state. For non-ideal quantum efficiency, it is possible for the detector to miscount the incoming photons, while for non-zero dark count, the detector may register extra photons even in the absence of a signal.

For 4QAM modulation, each two bits $x_1$ and $x_2$ are mapped to a coherent state signal, as shown in Fig. 1. The *a posteriori* log-likelihood ratios $\lambda_j^{post}(x_1)$ and $\lambda_j^{post}(x_2)$ of each information bit would be derived, respectively. For bit $x_1$, the *a posteriori* log-likelihood ratios are given by

$$\begin{aligned} \lambda_j^{post}(x_1) &= \ln \frac{P(I_m|x_1=1)}{P(I_m|x_1=0)} + \ln \frac{P(x_1=1)}{P(x_1=0)} \\ &= \lambda_j^e(x_1) + \lambda_j^a(x_1), \end{aligned} \quad (13)$$

where $\lambda_j^e(x_1)$ and $\lambda_j^a(x_1)$ denote the extrinsic log-likelihood ratio and the *a priori* log-likelihood ratio in interval $j$, respectively. According to the Bayesian Rule, the extrinsic log-likelihood ratio of bit $x_1$ can be rewritten as

$$\begin{aligned} \lambda_j^e(x_1) &= \ln \frac{P\left(I_{m,j}|x_1=1\right)}{P\left(I_{m,j}|x_1=0\right)} \\ &= \ln[P\left(I_{m,j}|x_1=1, x_2=0\right) P(x_2=0|x_1=1) \\ &\quad + P\left(I_{m,j}|x_1=1, x_2=1\right) P(x_2=1|x_1=1)] \\ &\quad - \ln[P\left(I_{m,j}|x_1=0, x_2=0\right) P(x_2=0|x_1=0) \\ &\quad + P\left(I_{m,j}|x_1=0, x_2=1\right) P(x_2=1|x_1=0)]. \end{aligned} \quad (14)$$

Upon considering the fact that the random variables of the coded bits $x_1$ and $x_2$ are independent, we have $P(x_2|x_1) = P(x_2)$, yielding

$$\begin{aligned} \lambda_j^e(x_1) &= \ln[P\left(I_{m,j}|x_1=1, x_2=0\right) P(x_2=0) \\ &\quad + P\left(I_{m,j}|x_1=1, x_2=1\right) P(x_2=1)] \\ &\quad - \ln[P\left(I_{m,j}|x_1=0, x_2=0\right) P(x_2=0) \\ &\quad + P\left(I_{m,j}|x_1=0, x_2=1\right) P(x_2=1)] \\ &= \ln\{P\left(I_{m,j}|x_1=1, x_2=0\right) \\ &\quad + P\left(I_{m,j}|x_1=1, x_2=1\right) \exp\left[\lambda_j^a(x_2)\right]\} \\ &\quad - \ln\{P\left(I_{m,j}|x_1=0, x_2=0\right) \\ &\quad + P\left(I_{m,j}|x_1=0, x_2=1\right) \exp\left[\lambda_j^a(x_2)\right]\}. \end{aligned} \quad (15)$$

Upon substituting (10) into (13), we arrive at

$$\lambda_j^e(x_1) = \ln \frac{\exp\left(\phi_{2,j}\right) + \exp\left[\phi_{4,j} + \lambda_j^a(x_2)\right]}{\exp\left(\phi_{1,j}\right) + \exp\left[\phi_{3,j} + \lambda_j^a(x_2)\right]}, \quad (16)$$

where $\phi_{m,j} = n_j \ln\left(\nu + \eta I_{m,j}\right) - \left(\nu + \eta I_{m,j}\right)$. Using the Jacobian logarithm [29] we arrive at the simple max-log approximation:

$$\begin{aligned} \lambda_j^e(x_1) &= \max\left\{\phi_{2,j}, \phi_{4,j} + \lambda_j^a(x_2)\right\} \\ &\quad - \max\left\{\phi_{1,j}, \phi_{3,j} + \lambda_j^a(x_2)\right\}. \end{aligned} \quad (17)$$

In a similar manner, the extrinsic log-likelihood ratio of bit $x_2$ can be derived as

$$\begin{aligned} \lambda_j^e(x_2) &= \max\left\{\phi_{3,j}, \phi_{4,j} + \lambda_j^a(x_1)\right\} \\ &\quad - \max\left\{\phi_{1,j}, \phi_{2,j} + \lambda_j^a(x_1)\right\}. \end{aligned} \quad (18)$$

Based on our iterative strategy of Fig. 3, the *a priori* information has to be fed back to the demapper/demodulator. For the first iterative detection, both the *a priori* log-likelihood $\lambda_j^a(x_1)$ and $\lambda_j^a(x_2)$ are set to be zero. The *a priori* probability $P_{prior\_m,1}$ satisfies

$$P_{porir\_m,1} = P_{porir\_x_1,1} \cdot P_{porir\_x_2,1}, \quad (19)$$

The *a posteriori* probability $P_{post\_m,j}$ can be calculated at the output of the demapper/demodulator. Upon substituting (10) into (13), the *a posteriori* log-likelihood ratio $\lambda_j^{post}(x_1)$ is given by

$$\lambda_j^{post}(x_1) = \ln \frac{P_{prior\_m=2,j} \cdot P_{m=2,j} + P_{prior\_m=4,j} \cdot P_{m=4,j}}{P_{prior\_m=1,j} \cdot P_{m=1,j} + P_{prior\_m=3,j} \cdot P_{m=3,j}}. \quad (20)$$

In a similar manner, the *a posteriori* log-likelihood ratio $\lambda_j^{post}(x_2)$ is given by

$$\lambda_j^{post}(x_2) = \ln \frac{P_{prior\_m=3,j} \cdot P_{m=3,j} + P_{prior\_m=4,j} \cdot P_{m=4,j}}{P_{prior\_m=1,j} \cdot P_{m=1,j} + P_{prior\_m=2,j} \cdot P_{m=2,j}}. \tag{21}$$

In the APP Decoder block of Fig. 3, the APP decoding is a standard function [30]. The *a priori* log-likelihood ratio $\lambda_j^a(x_1)$ and $\lambda_j^a(x_2)$ can be obtained from the *a posteriori* log-likelihood ratio $\lambda_j^{post}(x_1)$ and $\lambda_j^{post}(x_2)$ according to (13). By substituting $\lambda_j^{post}$ of (20), (21) and $\lambda_j^e$ of (17), (18) into (13), we arrive at:

$$\begin{aligned} \lambda_j^a(x_1) &= \lambda_j^{post}(x_1) - \lambda_j^e(x_1), \\ \lambda_j^a(x_2) &= \lambda_j^{post}(x_2) - \lambda_j^e(x_2). \end{aligned} \tag{22}$$

The output sequences $\lambda_j^a(x_1)$ and $\lambda_j^a(x_2)$ are then used for calculating $\lambda_j^e(x_1)$ and $\lambda_j^e(x_2)$ in (17) and (18) for the next iteration. Then $m^*$ of the local field $|\beta_{m^*,j}\rangle$ can be obtained via the maximum *a posteriori* (MAP) rule. The $m^*$ of the last interval corresponding to $\lambda_N^{post}$ becomes the hard-decision output $\tilde{d}$ shown in Fig. 3.

### B. GENERAL ITERATIVE SCHEME

So far we have concentrated our attention on 4QAM signals, we emphasize that we can generalize these receivers to M-ary QAM signals ($M > 4$), as shown in Fig. 4 and detailed below.

The split state is only partially affected by the receiver's quantum impairments and not all the parts are equally badly affected, hence we can achieve beneficial gains by iteratively exchanging information among them. In the APP decoder, the APP decoder of [30] is invoked for determining the *a priori* log-likelihood ratio $\lambda_j^a$ and the information bits $\tilde{d}_j$ recovered from the extrinsic log-likelihood ratio $\lambda_j^e$. For soft signal detection, the decoder makes a decision based on the number of photons in the specific slot having the maximum soft value of the signal. In the iterative feedback block of Fig. 3, the maximum *a posteriori* soft detection is invoked [30] and the soft output (usually the log-likelihood ratio of each bit) gleaned from the soft demapper/demodulator is fed back to the APP decoder for improving the error probability

For $M$-ary QAM modulation, each of the attained $K = log_2 M$ bits is mapped to a coherent state signal. The *a posteriori* log-likelihood ratio $\lambda_j^{post}$ of the $k^{th}$ bit would be derived according to

$$\begin{aligned} \lambda_j^{post}(x_k) &= ln \frac{P(x_k = 1|I_{m,j})}{P(x_k = 0|I_{m,j})} \\ &= \ln \frac{P(I_{m,j}|x_k = 1)}{P(I_{m,j}|x_k = 0)} + \ln \frac{P(x_k = 1)}{P(x_k = 0)} \\ &= \lambda_j^e(x_k) + \lambda_j^a(x_k), \end{aligned} \tag{23}$$

where $\lambda_j^e(x_k)$ and $\lambda_j^a(x_k)$ represent the extrinsic log-likelihood ratio and the *a priori* log-likelihood ratio of the $k$th bit in interval $j$, respectively.

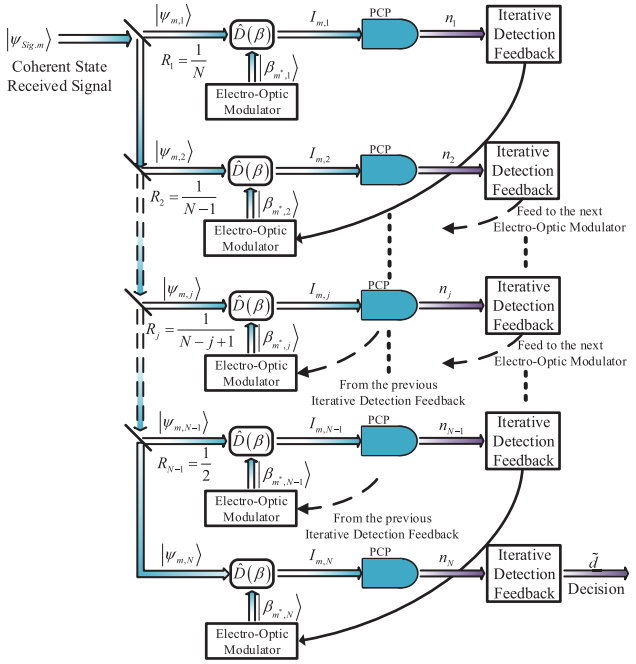


**FIGURE 4.** The schematic of the soft iterative quantum receiver. The diagonal lies at the input represent the beam splitters. $\hat{D}(\beta)$ is the displacement operate and the PCP represents the photon-counting process using the PNRD.

Upon considering the fact that the random variables representing each of the $k$ coded bits are independent, we have

$$\lambda_j^e(x_k) = \ln \frac{\sum_{k'=0,k'\neq k}^{K-1} P\left(I_{m,j}|x_k = 1, x_{k'}\right) P(x_{k'})}{\sum_{k'=0,k'\neq k}^{K-1} P\left(I_{m,j}|x_k = 0, x_{k'}\right) P(x_{k'})}. \tag{24}$$

Similar arguments to those of the previous section can be applied to $M$-ary QAM. Let

$$\phi_{m,j} = n_j \ln\left(\nu + \eta I_{m,j}\right) - \left(\nu + \eta I_{m,j}\right), \quad m = 1, \cdots, M. \tag{25}$$

Then using the Jacobian logarithm, the extrinsic log-likelihood ratio of each information bit can be expressed in the form of (17) and (18). Then for $M$-ary QAM we have

$$\lambda_j^e(x_k) = \max_{x_k=1}\left\{\phi_{k,j} + \lambda_{k,j}^a\right\} - \max_{x_k=0}\left\{\phi_{k,j} + \lambda_{k,j}^a\right\}. \tag{26}$$

The *a posteriori* log-likelihood ratio $\lambda_j^{post}(x_k)$ is given by

$$\lambda_j^{post}(x_k) = \ln \frac{\sum_{m:x_k=1} P_{prioir\_m,j} \cdot P_{m,j}}{\sum_{m:x_k=0} P_{prioir\_m,j} \cdot P_{m,j}}, \tag{27}$$

where $m : x_k = 1$ and $m : x_k = 0$ represent the index of the $M$-ary QAM alphabet when $x_k = 1$ or $x_k = 0$. The *a priori* log-likelihood ratio can be formulated as

$$\lambda_j^a(x_k) = \lambda_j^{post}(x_k) - \lambda_j^e(x_k). \tag{28}$$

The iterative detection algorithm can be summarized as Algorithm 1 for the sake of explicit clarity.

**Algorithm 1** Iterative Detection Algorithm

1) **Initialization:**Split the received signal into $N$ parts, let $\left|\beta_{m*,1}\right\rangle = \left|\psi_{Sig.0}\middle/\sqrt{N}\right\rangle$.
2) **Main iteration**
a) Operate the displacement operator $\hat{D}(\beta)$ on the received state $\left|\psi_{m,j}\right\rangle$ with the local field $\left|\beta_{m^*,j}\right\rangle$ according to (6).
b) Measure the displaced state with measurement operator $\hat{\Pi}_n$ using PNRD according to (8).
c) Calculate $P_{post\_m,j}$ and $\lambda_j^{post}$ according to (10) and (27).
d) Calculate $\lambda_j^e$ according to (26) and update $\lambda_j^a$ according to (28).
e) After a number of iterations, calculate the $m^*$ according to the MAP rule.
3) **Hard decision:** After all splite state is detected, the recovered bit $\tilde{d}$ is obtained subject to the hard decision in the last part.

In the presence of $N$ time-intervals and of the PNRD detector's imperfections, it is challenging to analytically study the performance of the proposed quantum receiver. Therefore, Monte Carlo simulations will be used for analyzing both the convergence behavior and the bit-error-ratio (BER) performance of the iterative receiver.

## IV. SIMULATION RESULTS

In this section, we characterize our iterative quantum receiver and compare its BER performance to that of the recently proposed non-iterative quantum receivers of [20] and [21]. Explicitly, the non-ideal quantum efficiency and the dark count of the photon detector, as well as the mode mismatch between the signal and the local oscillating field will be compared between our iterative receiver and the receivers of [20] and [21]. Moreover, we use EXIT charts to study the convergence behaviour of the iterative receiver [25].

The minimum error probability achieved by the optimum detection of both PSK and QAM have been given in [31]. The square root measurement (SRM) achieves the minimum error probability with the aid equal *a priori* probability. When the SRM is adopted, the error probability is represented as

$$P_e = 1 - \frac{1}{M^2}\left(\sum_{l=1}^{M}\sqrt{\lambda_l}\right)^2, \tag{29}$$

where $\lambda_l$ is the eigenvalue of the Gram matrix.

### A. ERROR PROBABILITY COMPARISON

Fig. 5 illustrates the BER performance of the iterative quantum receiver and of the recently proposed non-iterative quantum receiver of [20] for 4QAM with different ratios of $R = N/M = 1.25$ and $R = N/M = 2.5$ [20], together with the SQL and the HL. Our simulation results indicate that the iterative receiver outperforms the conventional non-iterative

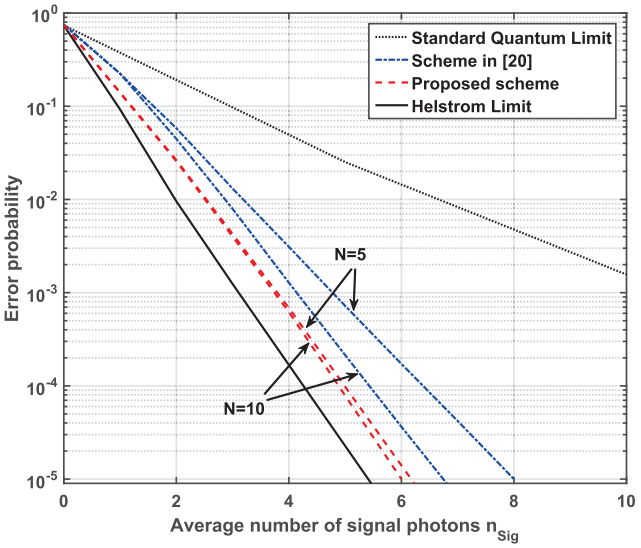


**FIGURE 5.** Error probability of both the iterative receiver and of the conventional non-iterative receiver for 4QAM.

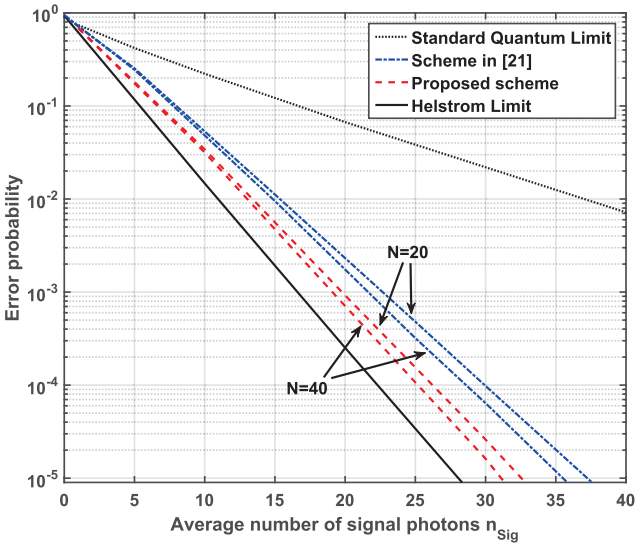


**FIGURE 6.** Error probability of both the iterative receiver and of the conventional non-iterative receiver for 16QAM.

quantum receiver. As the number of intervals $N$ increases, the BER performance of both the proposed scheme and of the receiver of [20] improves. However, for a fixed number of intervals $N$, the error probability of the iterative receiver shows a better performance than the receiver of [20] and approaches the HL more closely.

Observe in Fig. 5 that, even in case of a lower intervals $N$ ($N = 5$ for the proposed receiver and $N = 10$ for the receiver in [20]), the BER of the proposed receiver exceeds that of the conventional non-iterative receiver. Explicitly, the proposed iterative strategy drastically improves the BER performance.

Furthermore, the BER of the iterative receiver and the receiver of [21] is depicted for 16QAM in Fig. 6. For this higher-order modulation, the BER performance of quantum receivers is more susceptible to the specific value of

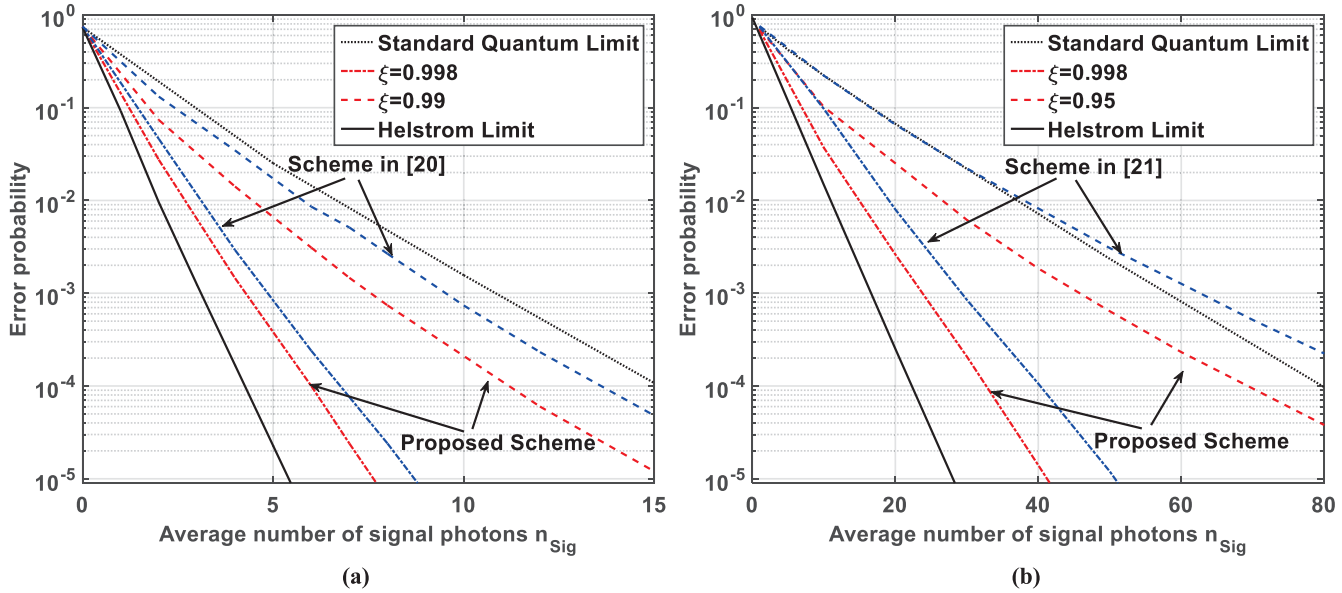


**FIGURE 7.** Error probability of the iterative receiver and the conventional non-iterative receiver under different mode mismatch for (a) 4QAM (b) 16QAM.

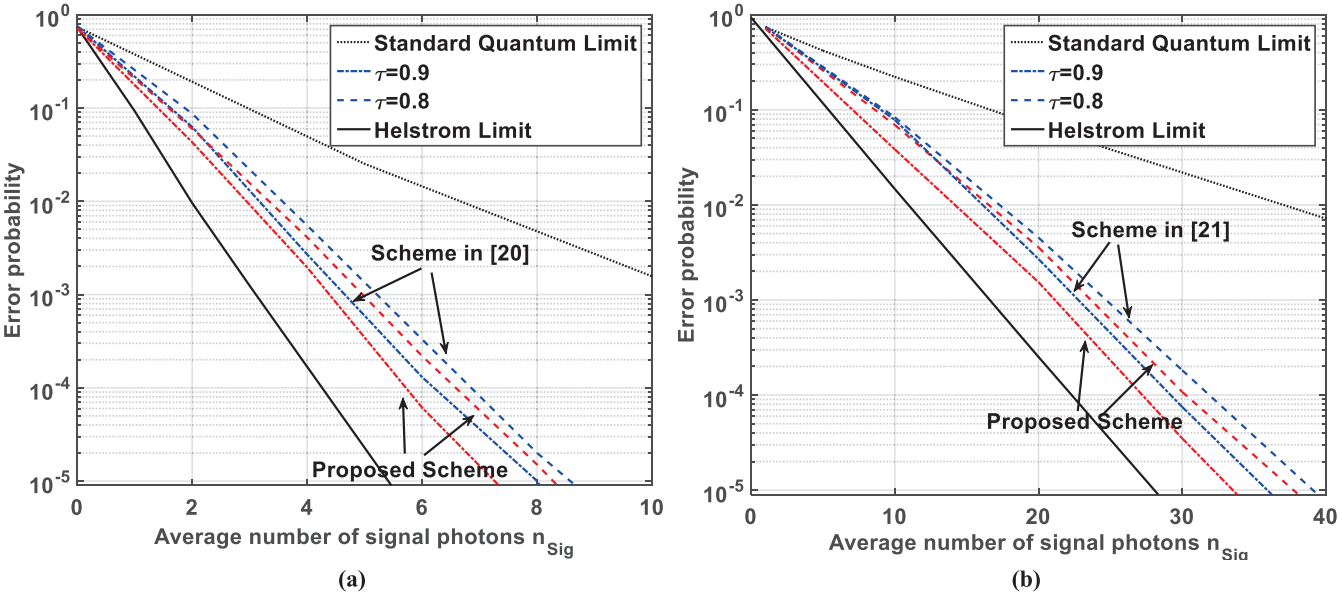


**FIGURE 8.** Error probability of the iterative receiver and the conventional non-iterative receiver under different transmittance for (a) 4QAM (b) 16QAM.

intervals $N$ due to the increased size of the signal alphabet. The proposed receiver achieves an approximately 1.05dB gain and approaches the HL for 16QAM with $N = 40$. Indeed, the proposed receiver remains superior to the conventional non-iterative receiver [21] even for $N = 20$. Meanwhile, the results of Fig. 6 suggest that $N$ may be reduced with the aid of our iterative strategy, which achieves a low BER, because the iterations extract as much information from each photon's arrival as possible. This is why our iterative strategy allows the quantum receiver to have an exceptional BER performance for M-ary QAM.

### B. ROBUSTNESS OF THE RECEIVER

Until now, all components of the channel and the receiver have been assumed to be ideal. In practice, however, diverse imperfections degrade the BER [16]. In this section, we will investigate the robustness of the iterative quantum receiver against several typical quantum-domain imperfections. In order to make a fair comparison with the benchmarkers, the same parameters were chosen. We consider the performance under the conditions of [19] including: (1) sub-unity mode mismatch $\xi$ between the signal and the local oscillating fields, (2) sub-unity transmittance $\tau$ of the

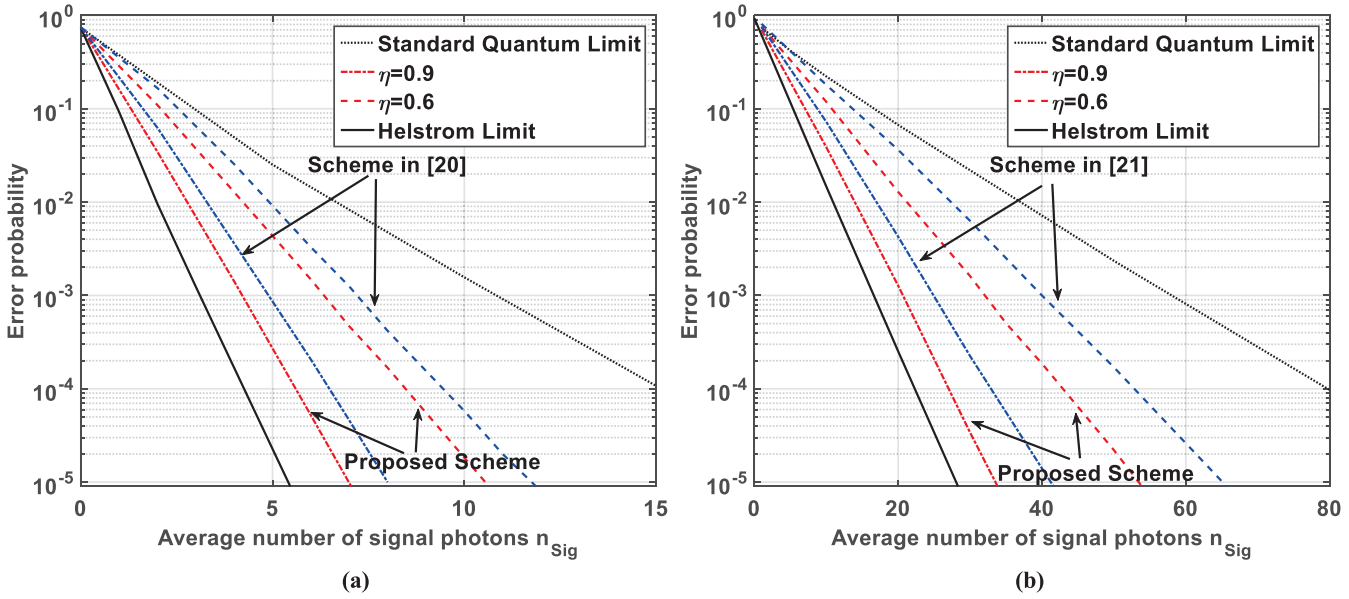


**FIGURE 9.** Error probability of the iterative receiver and the conventional non-iterative receiver under different quantum efficiency for (a) 4QAM (b) 16QAM.

beam splitter, (3) non-ideal quantum efficiency $\eta$, where it is possible for the detector to miscount incoming photons, (4) non-zero dark count $\nu$, where the detector may register photon arrivals even in the absence of a signal. Monte Carlo simulations of the iterative receivers and of the non-iterative receivers were performed to compare the impact of these individual imperfections.

The traces seen in Fig. 7 and Fig. 8 have been adjusted to account for some typical values of $\xi$ and $\tau$. For example, $\xi = 0.998$ represents a minor mode mismatch; $\xi = 0.99$ and $\xi = 0.95$ are typical situations achieved in previously documented experiments [27]. The measured error probability versus average photon count for the transmittance of $\tau = 0.9$ and $\tau = 0.8$ is depicted in Fig.8. Due to the mode mismatch and sub-unity transmittance, the BER performance of both the iterative receiver and of the non-iterative receiver [20], [21] deteriorates to some extent. For the receivers in [20] and [21], the BER performance is seriously degraded even with a minor mode mismatch. Most significantly, the BER performance of the iterative receiver remains better than the SQL, while that of the receivers in [21] is worse than the SQL, when $\xi = 0.95$. It becomes evident that the degradation of the iterative receiver is less severe than that of the receivers of [20] and [21], illustrating that the deleterious effects of mode mismatch or sub-unity transmittance are mitigated by our iterative strategy.

In Fig. 9 and Fig. 10, we discuss the BER performance under detector imperfections. The typical imperfections imposed by non-ideal quantum efficiency $\eta$ and by dark count $\nu$ are investigated. For comparison, the BER performance of both the iterative receiver and of the non-iterative receiver having a quantum efficiency of $\eta = 0.9$ and $\eta = 0.6$ are plotted in Fig. 9. For higher-order modulation, non-ideal quantum efficiency will impose a significant performance degradation on the receiver of [21], since it results in a failure mode, where the *a priori* probability becomes incorrect. The conventional non-iterative receiver of both 4QAM and 16QAM becomes quite susceptible to the quantum efficiency degradation. Even upon considering a quantum efficiency $\eta = 0.6$, the proposed receiver significantly outperforms the conventional 16QAM non-iterative receiver, explicitly illustrating that the errors due to non-ideal quantum efficiency can be mitigated by our iterative strategy.

The measured BER versus the average number of photons for a dark count of $\nu = 10^{-5}$ and $\nu = 10^{-2}$ is depicted in Fig.10. The BER performance of the receivers in [20] and [21] exhibits a floor, which suggests that the dark count seriously limits the performance of the non-iterative quantum receivers, when having relatively higher photon counts. By contrast, the performance of the iterative quantum receiver is degraded modestly, which is free from the above-mentioned BER floor formation. It should be noted that the dark count has a stronger impact on the BER performance than the quantum efficiency.

In the case of a quantum receiver relying on the nulling of the probed states, the dark count will simply add to the photon count of the optical signal and will lead to deleterious effects. This results in interference between the amplitude of the local field $|\phi_{m^*,j}\rangle$ and the signal $|\phi_{Sig,m}\rangle$. The imperfection of the detector strongly distorts the signal constellations and results in an increased BER. However, the performance degradation remains more moderate for our iterative strategy.

### C. EXIT CHART ANALYSIS

The EXIT chart is applied for visualizing the convergence behavior of the proposed iterative block. The iterative

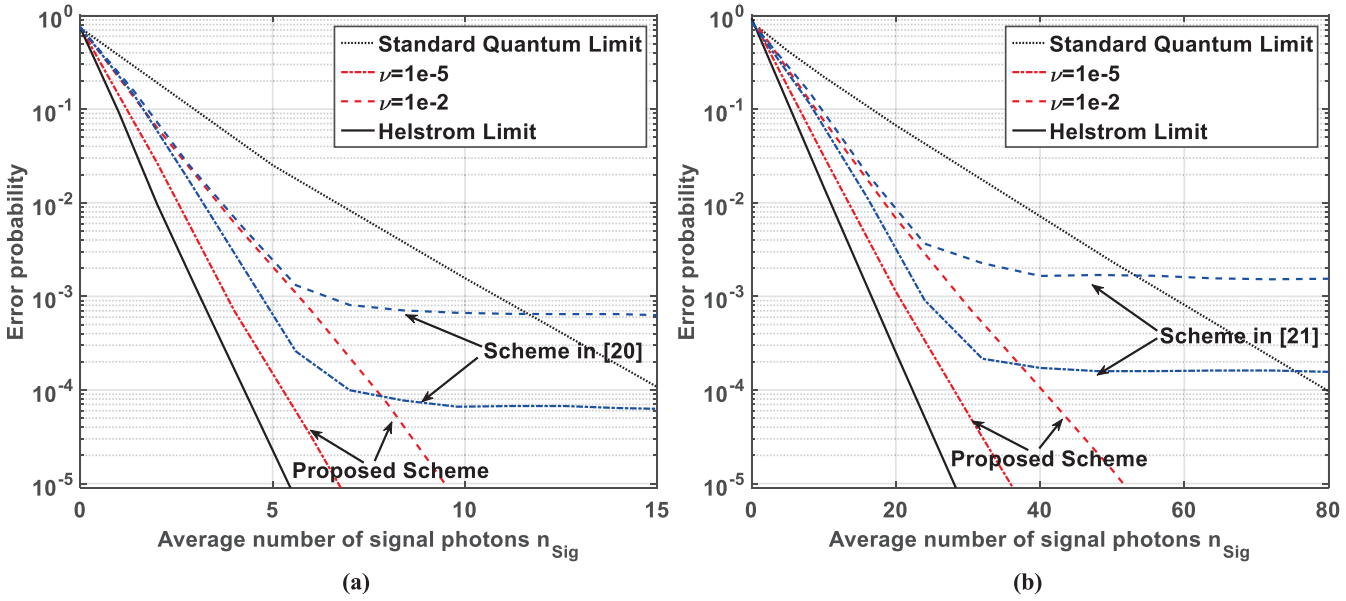


**FIGURE 10.** Error probability of the iterative receiver and the conventional non-iterative receiver under different dark count for (a) 4QAM (b) 16QAM.

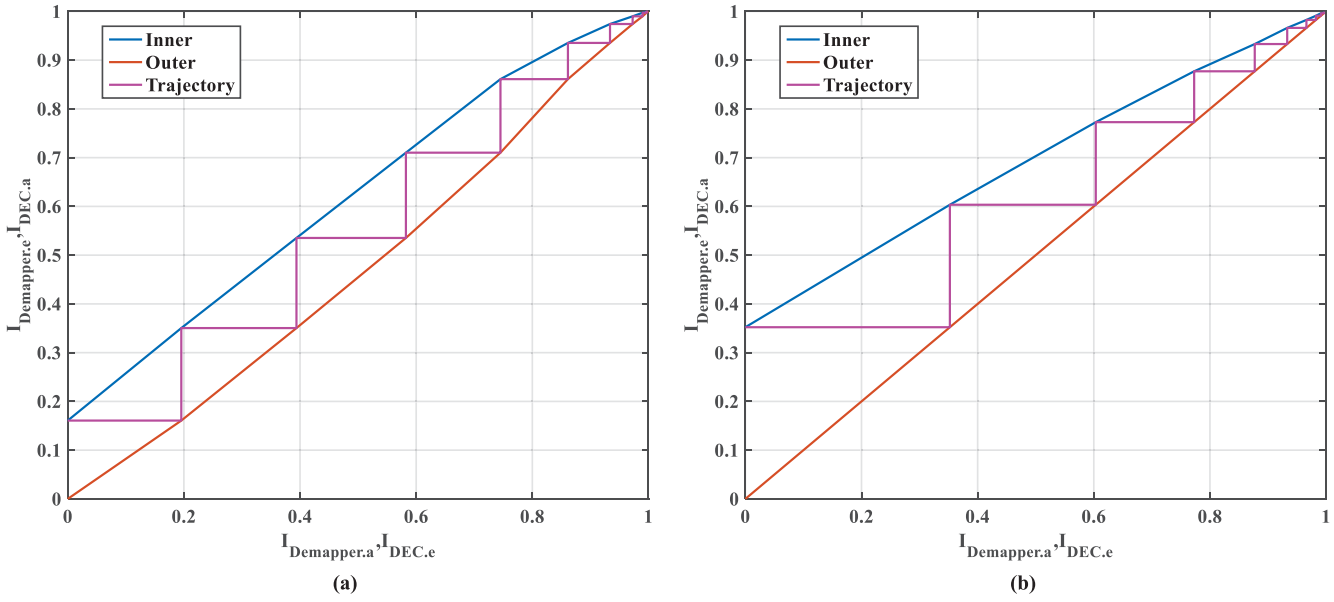


**FIGURE 11.** The EXIT chart of the iterative receiver for (a) 4QAM (b) 16QAM.

detection feedback block in the proposed scheme process the traditional information, which could be analyzed by EXIT chart [32]. In this section, familiarity with EXIT chart analysis is assumed [25]. The exchange of extrinsic information can be visualized by the stair-case-shaped decoding trajectory seen in Fig. 11 for 4QAM in conjunction with $n_{Sig} = 5$ and 16QAM with $n_{Sig} = 25$. The reason for the selection of the average signal photon count $n_{Sig}$ is that the EXIT chart analysis characterizes the iterative detection performance, where a moderate signal energy is selected. In Fig. 11 the blue curve indicates the mutual information improvement of the inner detection component, while the red curve indicates that of the outer receiver component. Each step of the stair-cased shaped trajectory indicates the mutual information improvement upon an extra iteration. For example, for the 4QAM scenario seen at the left eight iterations are required for approaching the 1:1 point, where an *a priori* information of 1 also results in an *a posteriori* information of one, which hence leads to high-confidence decisions associated with a low error probability. The number of iterations required for 16QAM to converge is higher than that of 4QAM due to the vulnerable nature of the higer-order modulation. It is also observed that

after a certain number of iterations, the mutual information improvements become marginal, illustrating that the iterative quantum receiver converges for both 4QAM and 16QAM. Some further properties of the EXIT-chart are, as detailed in [32]:

(1) The area under the inner decoder's curve is proportional to the achievable throughput of the system;
(2) The area between the inner and outer component's curves is representative of how close the system is capable of operating to its capacity. A narrow open tunnel between them corresponds to near-capacity operation.

## V. CONCLUSIONS

We have improved the state-of-the-art quantum receiver. Explicitly, an iterative quantum receiver was proposed for QAM signals. The classical quantum receivers simply use the Bayesian updating procedure and we improve it using the soft iterative detection. The BER performance, robustness as well as mutual information evolution of iterative quantum receiver were analyzed. The iterative receiver has the potential of identifying and mitigating the effects of practical quantum-domain impairments, especially the fidelity degradation due to dark counts. Hence our iterative receivers are capable of approaching the Helstrom limit. We also demonstrate that the iterative receiver is capable of achieving an exceptional error performance at a reduced number of feedback steps. Fewer feedback steps will allow us to detect a shorter pulse width or higher rate signals, which are important for demanding practical applications. In conclusion, our iteration-based quantum receiver is capable of outperforming the state-of-art quantum solutions.

## REFERENCES

[1] P. Botsinis, S. X. Ng, and L. Hanzo, "Quantum search algorithms, quantum wireless, and a low-complexity maximum likelihood iterative quantum multi-user detector design," *IEEE Access*, vol. 1, pp. 94–122, 2013.
[2] G. Li, "Coherent optical technologies for free-space optical communication and sensing," in *Proc. Appl. Lasers Sens. Free Space Commun.*, 2011, p. LTuD1.
[3] S. Izumi, M. Takeoka, K. Wakui, M. Fujiwara, K. Ema, and M. Sasaki, "Optical phase estimation via the coherent state and displaced-photon counting," *Phys. Rev. A, Gen. Phys.*, vol. 94, no. 3, p. 033842, 2016.
[4] R. S. Kennedy, "A near-optimum receiver for the binary coherent state quantum channel," MIT Res. Lab. Electron., Massachusetts Inst. Technol., Cambridge, MA, USA, Tech. Rep. 108, 1973.
[5] S. J. Dolinar, "An optimum receiver for the binary coherent state quantum channel," MIT Res. Lab. Electron., Massachusetts Inst. Technol., Cambridge, MA, USA, Tech. Rep. 111, 1973.
[6] R. L. Cook, P. J. Martin, and J. M. Geremia, "Optical coherent state discrimination using a closed-loop quantum measurement," *Nature*, vol. 446, no. 7137, pp. 774–777, 2007.
[7] K. Tsujino *et al.*, "Quantum receiver beyond the standard quantum limit of coherent optical communication," *Phys. Rev. Lett.*, vol. 106, no. 25, p. 250503, 2011.
[8] K. Tsujino *et al.*, "Sub-shot-noise-limit discrimination of on-off keyed coherent signals via a quantum receiver with a superconducting transition edge sensor," *Opt. Exp.*, vol. 18, no. 8, pp. 8107–8114, 2010.
[9] F. E. Becerra, J. Fan, G. Baumgartner, J. Goldhar, J. T. Kosloski, and A. Migdall, "Experimental demonstration of a receiver beating the standard quantum limit for multiple nonorthogonal state discrimination," *Nature Photon.*, vol. 7, no. 2, pp. 147–152, 2013.
[10] C. W. Helstrom, "Quantum detection and estimation theory," *J. Statist. Phys.*, vol. 1, no. 2, pp. 231–252, 1969.
[11] R. S. Bondurant, "Near-quantum optimum receivers for the phase-quadrature coherent-state channel," *Opt. Lett.*, vol. 18, no. 22, pp. 1896–1898, 1993.
[12] S. Izumi *et al.*, "Displacement receiver for phase-shift-keyed coherent states," *Phys. Rev. A, Gen. Phys.*, vol. 86, no. 4, p. 042328, 2012.
[13] C. R. Müller *et al.*, "Quadrature phase shift keying coherent state discrimination via a hybrid receiver," *New J. Phys.*, vol. 14, no. 8, p. 083009, 2012.
[14] C. Wittmann, M. Takeoka, K. N. Cassemiro, M. Sasaki, G. Leuchs, and U. L. Andersen, "Demonstration of near-optimal discrimination of optical coherent states," *Phys. Rev. Lett.*, vol. 101, no. 21, p. 210501, 2008.
[15] M. Takeoka and M. Sasaki, "Discrimination of the binary coherent signal: Gaussian-operation limit and simple non-Gaussian near-optimal receivers," *Phys. Rev. A, Gen. Phys.*, vol. 78, no. 2, p. 022320, 2008.
[16] C. R. Müller and C. Marquardt, "A robust quantum receiver for phase shift keyed signals," *New J. Phys.*, vol. 17, no. 3, p. 032003, 2015.
[17] C. Wittmann, U. L. Andersen, M. Takeoka, D. Sych, and G. Leuchs, "Demonstration of coherent-state discrimination using a displacement-controlled photon-number-resolving detector," *Phys. Rev. Lett.*, vol. 104, no. 10, p. 100505, 2010.
[18] F. E. Becerra *et al.*, "$M$-ary-state phase-shift-keying discrimination below the homodyne limit," *Phys. Rev. A, Gen. Phys.*, vol. 84, no. 6, p. 062324, 2011.
[19] J. M. Geremia, "Distinguishing between optical coherent states with imperfect detection," *Phys. Rev. A, Gen. Phys.*, vol. 70, no. 6, p. 062303, 2004.
[20] K. Li, Y. Zuo, and B. Zhu, "Suppressing the errors due to mode mismatch for $M$-ary PSK quantum receivers using photon-number-resolving detector," *IEEE Photon. Technol. Lett.*, vol. 25, no. 22, pp. 2182–2184, Nov. 15, 2013.
[21] Y. Zuo, K. Li, and B. Zhu, "16-QAM quantum receiver with hybrid structure outperforming the standard quantum limit," in *Proc. MATEC Web Conf.*, 2016, pp. 1–4.
[22] V. A. Vilnrotter, "Quantum receiver for distinguishing between binary coherent-state signals with partitioned-interval detection and constant-intensity local lasers," NASA, Washington, DC, USA, IPN Prog. Rep. 42-189, 2012.
[23] J. Chen, J. L. Habif, Z. Dutton, R. Lazarus, and S. Guha, "Optical codeword demodulation with error rates below the standard quantum limit using a conditional nulling receiver," *Nature Photon.*, vol. 6, no. 6, pp. 374–379, 2012.
[24] S. ten Brink, "Convergence behavior of iteratively decoded parallel concatenated codes," *IEEE Trans. Commun.*, vol. 49, no. 10, pp. 1727–1737, Oct. 2001.
[25] L. Hanzo, T. H. Liew, B. L. Yeap, R. Y. S. Tee, and S. X. Ng, *Turbo Coding, Turbo Equalisation and Space-Time Coding: EXIT-Chart-Aided Near-Capacity Designs for Wireles*. Hoboken, NJ, USA: Wiley, 2011.
[26] S. M. Barnett, L. S. Phillips, and D. T. Pegg, "Imperfect photodetection as projection onto mixed states," *Opt. Commun.*, vol. 158, nos. 1–6, pp. 45–49, 1998.
[27] S. Izumi, M. Takeoka, K. Ema, and M. Sasaki, "Quantum receivers with squeezing and photon-number-resolving detectors for M-ary coherent state discrimination," *Phys. Rev. A, Gen. Phys.*, vol. 87, no. 4, p. 042328, 2013.
[28] F. E. Becerra, J. Fan, and A. Migdall, "Photon number resolution enables quantum receiver for realistic coherent optical communications," *Nature Photon.*, vol. 9, no. 1, pp. 48–53, 2015.
[29] J. Erfanian, S. Pasupathy, and G. Gulak, "Reduced complexity symbol detectors with parallel structure for ISI channels," *IEEE Trans. Commun.*, vol. 42, no. 234, pp. 1661–1671, Apr. 1994.
[30] C. Berrou and A. Glavieux, "Near optimum error correcting coding and decoding: Turbo-codes," *IEEE Trans. Commun.*, vol. 44, no. 10, pp. 1261–1271, Oct. 1996.
[31] K. Kato, M. Osaki, M. Sasaki, and O. Hirota, "Quantum detection and mutual information for QAM and PSK signals," *IEEE Trans. Commun.*, vol. 47, no. 2, pp. 248–254, Feb. 1999.
[32] M. El-Hajjar and L. Hanzo, "EXIT charts for system design and analysis," *IEEE Commun. Surveys Tuts.*, vol. 16, no. 1, pp. 127–153, 1st Quart., 2014.

**CHENJIA WEI** received the B.Eng. degree in communication engineering from the Nanjing University of Post and Telecommunication in 2016, where he is currently pursuing the M.Eng. degree in communication science and engineering with Fudan University. His current research interests includ quantum communications and wireless communications.

**XIAOLIN ZHOU** received the B.Eng. degree from the Department of Technical Physics, Xidian University, in 1996, the M.Eng. degree from the Nanjing University of Aeronautics and Astronautics in 1999, and the Ph.D. degree from Shanghai Jiao Tong University, China, in 2003. From 2005 to 2006, he was a Visiting Researcher at Monash University, Australia. He is currently an Associate Professor with the Department of Communication Science and Engineering, Fudan University, China. His research interests include quantum communications, free-space optical communications, and signal processing technology.

**LINGDA WANG** received the B.Eng. degree in electronic and information science and technology from Fudan University, Shanghai, China, in 2017. He is currently pursuing the M.Sc. degree in electrical and computer engineering with the University of Illinois at Urbana–Champaign, Urbana, IL, USA. His research interests include graph theory, community detection, machine learning, and quantum communications.

**PENGFEI TIAN** received the bachelor's degree from the Huazhong University of Science and Technology in 2007, the master's degree from Peking University in 2010, and the Ph.D. degree from the Institute of Photonics, University of Strathclyde, U.K., in 2014. He has been an Associated Professor with Fudan University since 2015. His research interests include quantum communications, micro-LED display, solid-state lighting, visible-light communications, and underwater optical wireless communications.

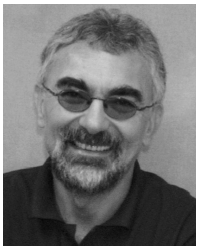

**LAJOS HANZO** (M'91–SM'92–F'04) received the D.Sc. degree in electronics in 1976 and the Ph.D. degree in 1983. During his 40-year career in telecommunications, he has held various research and academic posts in Hungary, Germany, and U.K. He was a Chaired Professor at Tsinghua University, Beijing. Since 1986, he has been with the School of Electronics and Computer Science, University of Southampton, U.K., where he holds the Chair in telecommunications. He is currently directing a 60-strong academic research team, working on a range of research projects in the field of wireless multimedia communications sponsored by industry, the Engineering and Physical Sciences Research Council, U.K., the European Research Council's Advanced Fellow Grant, and the Royal Society's Wolfson Research Merit Award. He is an enthusiastic supporter of industrial and academic liaison, and he offers a range of industrial courses. He has successfully supervised 111 Ph.D. students, co-authored 18 John Wiley/IEEE Press books on mobile radio communications totalling in excess of 10 000 pages, and published 1685 research contributions at the IEEE Xplore. He was a FREng, FIET, and fellow of the EURASIP. He received an Honorary Doctorate from the Technical University of Budapest in 2009 and The University of Edinburgh in 2015. In 2016, he was admitted to the Hungarian Academy of Science. He is a Governor of the IEEE VTS. He served as the TPC chair and the general chair of the IEEE conferences, presented keynote lectures, and has been received a number of distinctions. From 2008 to 2012, he was the Editor-in-Chief of the IEEE Press. He has over 30 000 citations and an H-index of 69.